

Retrieval methods of soil water content in vegetation covering areas based on multi-source remote sensing data

ZHOU Peng, DING Jianli, WANG Fei, Guljamal.Ubul, ZHANG Zhiguang

Lab for Oasis Ecosystem of Xinjiang, College of Resource and Environmental Science, Xinjiang University, Urumqi 830046, China

Abstract: This paper takes the delta oasis of Weigan and Kuqa rivers in Xinjiang as the study area. Fusion image of SAR (Radar-sat image) combined with visible spectrum remote sensing image (TM image) is used to extract soil and vegetation water content in arid oasis. Based on the Normalized Difference Moisture Index extracted from homochronous visible spectrum remote sensing data, this thesis utilizes “water-cloud model” to wipe off vegetation influence from total backscattering coefficient of radar data and sets up the relationship between soil backscattering coefficient and soil moisture. Correlation coefficient for HH Polarization is $R^2=0.5227$, for HV Polarization is $R^2=0.3277$. Result shows that in arid and semi-arid area where the main crops are cotton and corn, the combination of C- band HH polarization radar data with visible image performs well in the study of removing vegetation influence while retrieving soil water content in medium vegetated areas.

Key words: soil moisture, remote sensing, vegetable, backscatter coefficient, water-cloud model

CLC number: TP751.1 **Document code:** A

Citation format: Zhou P, Ding J L, Wang F, Guljamal.Ubul and Zhang Z G. 2010. Retrieval methods of soil water content in vegetation covering areas based on multi-source remote sensing data. *Journal of Remote Sensing*. **14**(5): 959—973

1 INTRODUCTION

Soil moisture is a very important component of the earth ecosystems, which is the tie of the surface water and ground-water. Soil moisture plays a very important role in the global water cycle, it is also an important parameter in the hydrological, meteorological and agricultural research (Yuan *et al.*, 2004). Large-scale soil moisture monitoring is an important content of agricultural water management and crop drought forecasting. At the same time, in regional and even the global-scale, soil moisture is also an essential parameter in the research of the land surface processes model, Which plays an important role in improving the regional and global climate models (Gao *et al.*, 2001). Recently, the monitoring of regional scale soil moisture helps to resolve the problems of hydrological model in arid drainage basin and monitor the growth of crops. Traditionally, the estimation of soil moisture requires intensive labour operations in the field and needs to do some complex post-treatment processes, which are not only time-consuming, but also difficult to obtain a wide range of synchronous soil moisture information. The development of remote sensing technology provides an effective means of accessing the regional scale soil moisture information (Cashion *et al.*, 2005; Urso & Minacapilli, 2006). At present, the methods of moni-

toring soil moisture based on remote sensing are mainly thermal inertia, thermal infrared, crop water stress index, anomalies of vegetation index and microwave remote sensing (Chen *et al.*, 1999; Guo & Zhao 2004). However, microwave remote sensing has the characters of all day and night, high repeated coverage, the penetrability through some surface objects and not restricted by weather conditions, which make microwave remote sensing monitoring of soil moisture widely used in arid and semi-arid area.

Soil moisture monitoring of microwave remote sensing has experienced 30-year history, and has been established many backscattering coefficient models such as small perturbation model, Kirchhoff model, two-scale model and the integral equation model and so on. In addition, there are experience and semi-empirical models (Baghdadi *et al.*, 2002; Liao *et al.*, 2002; Wickel *et al.*, 2001; Xiong & Shao, 2006). However, in the vegetated areas of arid and semi-arid oasis, the application of these retrieval models are confined by surface roughness and vegetation coverage. Higher vegetation coverage will cause lower estimation on soil moisture and the higher estimation on surface roughness (Liu *et al.*, 2005) which make the acquisition of soil moisture became complex. The key question to the study of soil moisture is how to eliminate the influence of surface roughness and separate the vegetation scattering and absorption

Received: 2009-11-20; **Accepted:** 2010-04-20

Foundation: Project of National Scientific Foundation of China (No. 40861020); the Open Fund of State Key Laboratory of Information Engineering in Surveying, Mapping and Remote Sensing (No. 09R03); Key Projects of Sciences Research of Education Ministry and Natural Science Foundation of XinJiang, China (No. 200821128).

First author biography: ZHOU Peng, (1980—), male, Post graduate of College of Resources and Environment Science, Xinjiang University, mainly engaged in the study of resources, environment and remote sensing application in arid area. E-mail: zp5226@hotmail.com

Corresponding author: DING Jianli, E-mail: watarid@xju.edu.cn

from the soil moisture. In these models, vegetation water content (VWC) is an important parameter. As it is very difficult to measure the parameter in the field, people usually use the optical image to predict and then establish the relationship between normalized difference moisture index (NDMI) and VWC. Based on the use of optical image data, this paper uses NDMI to estimate the study area's vegetation water content, then, employs multi-polarization satellite-based radar data together with microwave scattering Water-Cloud Model eliminating the impact of the vegetation layer and isolating the contributions of vegetation scattering and absorption from the total backscattering coefficient, Which is the research on the estimation of surface soil moisture in vegetated areas in arid oasis.

2 STUDY AREA AND DATA SOURCE

2.1 Status of study area

The study area in this paper locates in the north of Tarim Basin, the lower reaches of Weigan and Kuqa Rivers, the middle of Tianshan and the north of Taklamagan desert. The average elevation is 920—1100m, which belongs to land

warm-temperate zone extreme arid climate. The average annual evaporation is 2420.23 mm, the average annual precipitation is 43.1mm, and the ratio of evaporation to precipitation is about 54 to 1. The image range of study area is that the coordinate of east longitude is from 82°15' to 82°53' and north latitude is from 41°15' to 42°36', which is confirmed according to the samples in field. Farm belt is dominant in study area, and the types of vegetation is not complex and is mainly composed of cotton (55%) and corn (15%) combining with other halophytes shrubs and salt secretion plants such as Tamarix, bulrush, Populus euphratica and Alhagi sparsifolia Shap.

2.2 Status of satellite data

Radarsat-2 satellite was successfully launched in December 14, 2007 at space launch base in Kazakhstan's Baikonur, it can provide 11 kinds of beam patterns, the highest resolution is 3m, the maximum imaging width is 500 km, and the maximum data rate is 445.4Mb/s, the range of incidence angle is 10°—60°.

The C-Band can effectively extract soil moisture of 0—5cm soil layer. The primary parameters of RADARSAT-2 System are showed in Table 1.

Table 1 Primary parameters of RADARSAT-2 system

| Carrier frequency | Polarization mode | Bandwidth/MHz | Antenna dimension/m ² | Antenna quality/kg | Active antenna | Proposed isolation/dB |
|-------------------|-------------------|-------------------------|----------------------------------|--------------------|----------------|-----------------------|
| C-Band (5.405GHz) | HH, HV VH, VV | 11.6, 17.3, 30, 50, 100 | 15×1.5 | 750 | C-Band T/R | >25 |

The multi-polarization data of Radarsat-2 in September 10, 2008 is chosen in this study, and the polarization is HH and HV. The homochronous visible data is Landsat-5 TM data which includes mid-infrared and near-infrared band for calculating NDMI. The image of study area is as follows:

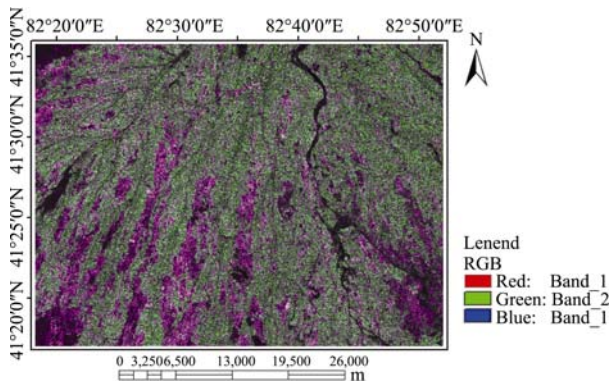


Fig. 1 Polarization composite image of RADARSAT 2 HH/HV

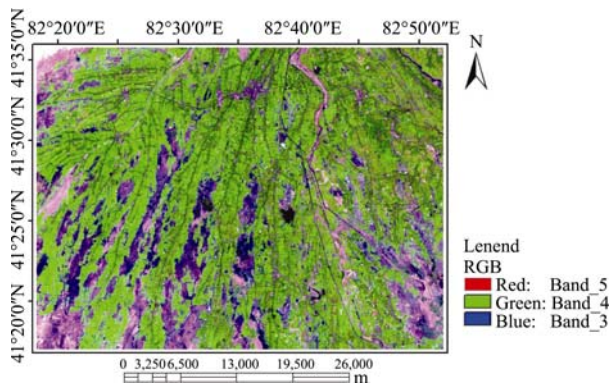


Fig. 2 RGB composite image of Landsat 5 TM 543

2.3 Collection and analysis of samples

In this study, Landsat-5 TM data obtained in Sep 27, 2007 is used as a reference map to choose the typical samples in the middle and the southwest of the oasis of Weigan and Kuqa rivers combining with GPS positioning technology. Sampling points are selected regularly distribution as much as possible and comprehensive considering of the local soil, vegetation type and other factors. Sampling time is from sep 16, 2008 to sep 26, 2008 and there are 30 located sampling points in this study. Set 5 sampling points as Plum-shape in the range of 30m of each located points and profile mining each sample points and the profiles of each sample are 0—5cm. Borrow these soil samples and vegetation samples around of the soil sample dots back to laboratories, and dry them with the weighing method to obtain the soil avoidupois moisture and vegetation water content.

3 PREPROCESSING

Image data pre-processing mainly includes image registration, geometric correction, noise reduction and color enhancement and so on. As it is need to find out the relationship between normalized difference moisture index (NDMI) and vegetation water content (VWC), the atmospheric correction of TM data is absolutely necessary. The level of SAR image data obtained is SLC, so it should do noise reduction, radiometric calibration and geometric correction.

3.1 Optical image processing

In order to keep the aboriginality, the image only did at-

atmospheric correction and geometric correction neglecting other pre-processing, which assure the objectivity of estimation. Because of the impacts of atmosphere on visible-near-infrared and thermal infrared are different, it is necessary to separately carry out atmospheric correction using 6S model (Liu & Zhao, 2002). While geometric correction was performed to do multinomial correction of TM image using ground control points.

3.2 Radar image processing

3.2.1 Radiometric calibration

As the radiometric error caused by the difference of the distance between ground scattering cell and radar, it is need to be corrected.

Radiometric calibration equations is :

$$\sigma^0 = \frac{D_n^2}{K} \sin(\alpha) \quad (1)$$

where, D_n^2 is the pixel intensity value, α is the radar incidence angle of the target location, K is the absolute calibration factor of the image. The values of K and α are obtained from the header files. SIGMA parameter correction is selected.

Figure out the distance orientational incident angle of every pixels, then RADARSAT-2 satellite image data is changed to backscattering coefficient using the below calibration expression:

$$\sigma^0(\theta) = 10 \log(D_n^2 + A_1) / A_2 + 10 \log(\sin(\theta)) \quad (2)$$

where, D_n is the gray-level value of radar image, A_1 , A_2 are automatic gain control coefficient of radar system, θ is the distance orientational incident angle of every pixels.

3.2.2 Noise treatment

The interrelated treatment in the processing of Radar-sat imaging causes a large number of spots (Speckle), which produce an obstacle on feature extraction, so the noise treatment is used to eliminate the impact. After several rounds of test analysis, 5×5 enhanced Lee filter to the original SAR image has the best filtering effect, which can eliminate the most spots.

3.2.3 Geometric calibration

In this thesis, the study area is flat, so cubic polynomial is selected as the correction method.

4 RETRIEVAL OF SOIL MOISTURE CONTENT IN VEGETATED AREAS

The vegetation water content (VWC) is extracted based on a choice of appropriate microwave scattering model. As it is definitely difficult to do large-scale area survey and extracting, which also definitely destroys vegetation, this paper uses Landsat-5 TM data to figure out normalized difference moisture index (NDMI) and find out the relationship between NDMI and VWC, then validates the vegetation water content. With that, multi-polarization satellite-based radar data together with microwave scattering water-cloud model are employed eliminating the impact of the vegetation layer on radar backscattering and finally retrieves the soil water content of study area.

4.1 Choice of microwave scattering model of soil moisture content in vegetated areas

In the study on soil moisture of Microwave remote sensing, vegetated areas will interfere with soilbacks cattering signal. Therefore, it is necessary to establish a rational vegetation scattering model and remove the impact of the vegetation in soil moisture retrieval algorithm. A lot of foreign scholars have been studied on vegetation scattering model: a group of Michigan State University in USA, proposed “MIMICS” Model in 1990, MIMICS Model (Fung *et al.*, 1992) was established for tall plants such as arbor, it took into account three levels of vegetation canopy, tree trunks and the bottom surface, which more realistically simulate the surface microwave backscattering. In 1978, Attma, Ulaby etc. using crops as the research object, proposed “Water-Cloud” model. “Water-Cloud” model assumes vegetation as homogeneous scatter and ignores the multiple scattering between vegetation layer and the surface. The overall backscattering of vegetation coverage area is simply divided into two parts, namely, the direct reflection by the vegetation back scattering and the ground backscattering after the double attenuation of crop.

Because there are mostly crops and other low vegetation in study area, “Water-Cloud” model is simple and practical. Besides, it uses very few parameters.

The model is expressed as follows:

$$\sigma_{can}^0(\theta) = \sigma_{veg}^0(\theta) + \gamma^2(\theta) \sigma_{soil}^0(\theta) \quad (3)$$

where, $\sigma_{can}^0(\theta)$ is the total radar backscattering coefficient in vegetated areas, $\sigma_{veg}^0(\theta)$ is the direct backscattering coefficient of vegetation layer, $\sigma_{soil}^0(\theta)$ is the direct backscattering coefficient of surface, $\gamma^2(\theta)$ is the double attenuation factor of radar wave penetrating crops, where:

$$\sigma_{veg}^0(\theta) = A \cdot m_{veg} \cdot \cos(\theta) \cdot (1 - \gamma^2(\theta)) \quad (4)$$

$$\gamma^2(\theta)_{pp} = \exp(-2Bm_{veg} \sec(\theta)) \quad (5)$$

In the expressions above, A and B are parameters depending on the type of vegetation which can be respectively obtained through regression arithmetic after the utilization of MIMICS model to simulate the surface parameters. m_{veg} is vegetation water content (kg/m^3), θ is the angle of incidence of radar wave.

4.2 Extracting of characteristic parameters and vegetation water content estimation

The vegetation water content is defined as the water content of plants per unit and per area. As a significant input parameter of Water-Cloud model, VWC performs very crucial effect on the retrieval of soil moisture in vegetated areas (Liu *et al.*, 2008). Now, the study of the regional retrieval of VWC using visible image has been already mature, and the relativity established between spectrum index and VWC is high (Jackson *et al.*,

2004; Rosnay *et al.*, 2006; Wang *et al.*, 2008). So, this study uses visible remote sensing to retrieve and field survey data of samples to validate the VWC in study area. In view of the spectrum characteristic of soil, vegetation and water between 0.8 to 1.7 μm , Landsat5 TM(sep 16,2008) homochronous with field survey date is chose which includes near- infrared band 4 (0.76 μm)and mid-infrared band 5(1.55 μm). The spectrum bandwidths are respectively 25 nm and 20 nm. According to the characteristic of vegetation that it has higher reflectivity in near-infrared band and lower reflectivity in mid-infrared band because of the absorbing effect of leave's water content, NDMI (Gao,1996; ZARCO-TEJADA *et al.*, 2003)is applied to extract vegetation water content information. As the vegetation in study area are most cotton and other low salt secretion plants, based on relevant research (Chen *et al.*, 2005), the equation is showed as expressions 6, while expressions 7 is established to gain VWC according to the relationship between vegetation water content of field survey and NDMI.

$$\text{NDMI} = (\text{NIR} - \text{MIR}) / (\text{NIR} + \text{MIR}) \quad (6)$$

$$\text{VWC} = 2.15\text{NDMI} + 0.32 \quad (7)$$

There are rivers, lakes and reservoirs in study area which disturb the extracting of vegetation water content. So, the effects of these water bodies must be removed in the process of the retrieval work. This paper uses MNDWI index (Xu, 2008) which is improved a little according as the regional circs to extract water body information, the equation is as follows:

$$\text{MNDWI} = (1+0.5)(\text{GREEN}-\text{MIR})/(\text{GREEN}+\text{MIR}) \quad (8)$$

After that, masking the original image and the water body effects are removed. Analysis and validation indicate that NDMI performs well in the retrieval of vegetation water content.

4.3 Calculating of backscattering in vegetated areas

The soil moisture estimation of initiative microwave remote sensing is mainly affected by vegetation coverage and surface roughness. The soil backscattering in vegetated area is composed of body scattering from vegetation, surface scattering from earth and the multiple scattering between vegetation layer and the surface. These factors are taken into account in the estimation of soil moisture content (Li *et al.*, 2002). As the hypsography in study area is flat, and mostly is covered by low plants, vegetation is considered seriously while the effect of surface roughness is not taken into account when calculating the soil backscattering coefficient.

In the study of soil moisture estimation in vegetated area, it is necessary to use "Water-Cloud" model to remove the contribution of vegetation in the backscattering. Parameters A and B are experience constants and they are changed by regional limit. A relatively mature method is applied to calibrate the parameters (Chen *et al.*, 2007; Gao *et al.*, 2008). Firstly, Water-Cloud and MIMICS model are used to simulate the backscattering coefficient of vegetated area then obtain the surface direct scattering and the variational relationship between surface scattering and incident angle. Follow that, parameters of the dominate plants in study area is showed in Table 2. Based on the simu-

lating results, calibrate the vegetation parameters A and B mentioned in Water-Cloud model through non-linear least squares method.

Table 2 Parameters input to MIMICS model

| Class | Parameters | Value |
|--------------|-----------------------------|-------|
| Sensor | Frequency /GHz | 5.4 |
| | Polarization mode | HH/HV |
| Land surface | Water content | 0.17 |
| | Root mean square height /cm | 0.817 |
| | Correlative length /cm | 7.528 |
| Leaves | Water content | 0.39 |
| | Radius /cm | 2.6 |
| | Thickness /cm | 0.04 |
| | Height /m | 0.9 |
| Branch | Radius /cm | 0.3 |
| | Length /cm | 21 |
| | Density /m ³ | 8.6 |
| Climate | Temperature /(°) | 22 |

After the analysis of regression, A is 0.0019 and B is 0.137. In term of Eq.(4) and Eq.(5), bare soil backscattering is acquired with Water-Cloud model removing the vegetation influence, the expressions are as follows:

$$\sigma_{\text{veg}}^0(\theta) = 0.0019 \times m_{\text{veg}} \times \cos(\theta) \times (1 - \gamma(\theta)^2) \quad (9)$$

$$\gamma^2(\theta) = \exp(-2 \times 0.137 m_{\text{veg}} \sec(\theta)) \quad (10)$$

$$\sigma_{\text{soil}}^0(\theta) = \frac{\sigma^0(\theta) - \sigma_{\text{veg}}^0(\theta)}{\gamma^2(\theta)} \quad (11)$$

The total backscattering coefficient of surface can be calculated from Eq. (2) and soil backscattering coefficient after eliminating vegetation effect is got from Eq.(11). In order to clear up the connection between HH and HV, there separately does a correlation analysis of backscattering coefficients of HH and HV before and after eliminating vegetation effect. Considering that the change of soil moisture can not be reflected effectively from radar backscattering coefficient in some high vegetated area, ambiguous dots are canceled in the analysis, results show:

Fig. 3 and Fig. 4 indicate that: whatever before or after eliminating vegetation effect, correlation coefficients of HH

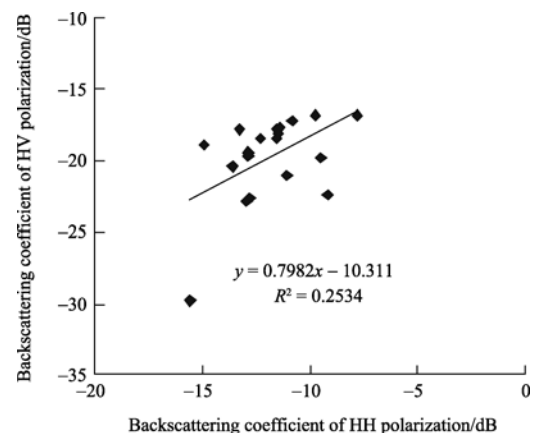


Fig. 3 Simulated curve between the backscattering coefficient of HH and HV polarization before eliminating vegetation effect

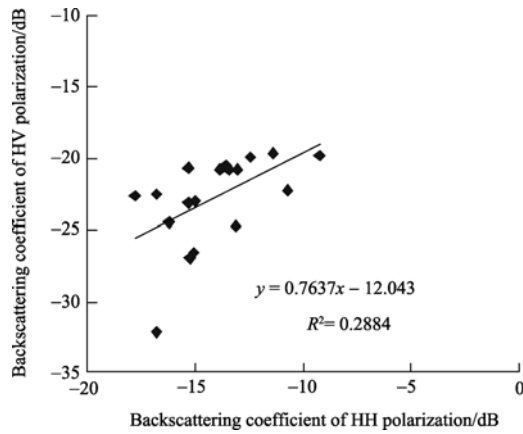


Fig. 4 Simulated curve between the backscattering coefficient of HH and HV polarization after eliminating vegetation effect

and HV polarization backscattering coefficients are all very low which are respectively 0.2534 and 0.2884. Therefore, the next work is to discuss the soil water content retrieval of HH, HV polarization.

4.4 Analysis of sample dots data

In order to analyze the effect factors of backscattering coefficient in vegetation coverage area, we got 30 sample dots from field survey which include water content in the soil layer of 0–5cm and the coordinates of these samples. Backscattering coefficient and water content of soil of the samples are showed in Table 3. According to the data in Table 3, respectively analyze the relationship between HH, HV polarization backscattering coefficient and water content of soil before and after removing vegetation influence and discuss the impact to backscattering coefficient of vegetation.

Table 3 Backscattering coefficient and water content of soil

| Samples | HH polarization /dB | HV polarization /dB | Water content in 5cm % |
|---------|------------------------|------------------------|---------------------------|
| C 1 | -13.2507 | -17.7713 | 5.1470 |
| C 2 | -10.7600 | -19.8877 | 4.9754 |
| C 3 | -11.5946 | -18.4416 | 5.0036 |
| C 4 | -11.3997 | -17.6153 | 8.4150 |
| C 5 | -12.2587 | -18.4515 | 7.6217 |
| C 6 | -12.5959 | -15.7758 | 14.7993 |
| C 7 | -11.5938 | -17.8194 | 11.7455 |
| C 8 | -10.7801 | -17.2293 | 13.1799 |
| C 9 | -14.3954 | -19.3163 | 3.6656 |
| C 10 | -9.6117 | -21.0139 | 10.7864 |
| C 11 | -12.8598 | -19.3812 | 4.3598 |
| C 12 | -15.9316 | -17.5230 | 3.2380 |
| C 13 | -14.9207 | -18.9558 | 2.2208 |
| C 14 | -9.7728 | -16.7673 | 18.8682 |
| C 15 | -7.8132 | -16.7763 | 20.1818 |
| C 16 | -13.1535 | -17.9993 | 12.1819 |
| C 17 | -12.8540 | -19.6966 | 4.9591 |
| C 18 | -14.1582 | -16.0084 | 4.1625 |
| C 19 | -13.8883 | -19.6414 | 4.0697 |
| C 20 | -13.5933 | -20.4478 | 4.8147 |
| C 21 | -12.8223 | -22.6523 | 3.1433 |
| C 22 | -10.5719 | -29.8080 | 1.1135 |
| C 23 | -9.2110 | -22.3394 | 6.7921 |
| C 24 | -8.8493 | -22.0768 | 13.1973 |
| C 25 | -12.9640 | -22.8122 | 1.3152 |
| C 26 | -11.4630 | -18.0514 | 8.5359 |
| C 27 | -15.0914 | -14.8482 | 2.0410 |
| C 28 | -11.0910 | -20.9843 | 7.2859 |
| C 29 | -9.4889 | -19.7483 | 15.7987 |
| C 30 | -8.8780 | -19.6783 | 10.3772 |

Obtain the corresponding backscattering coefficient of the 30 samples in the image according as their coordinates, the relationship between before and after removing vegetation influence of HH, HV polarization backscattering coefficient displayed in Fig. 5.

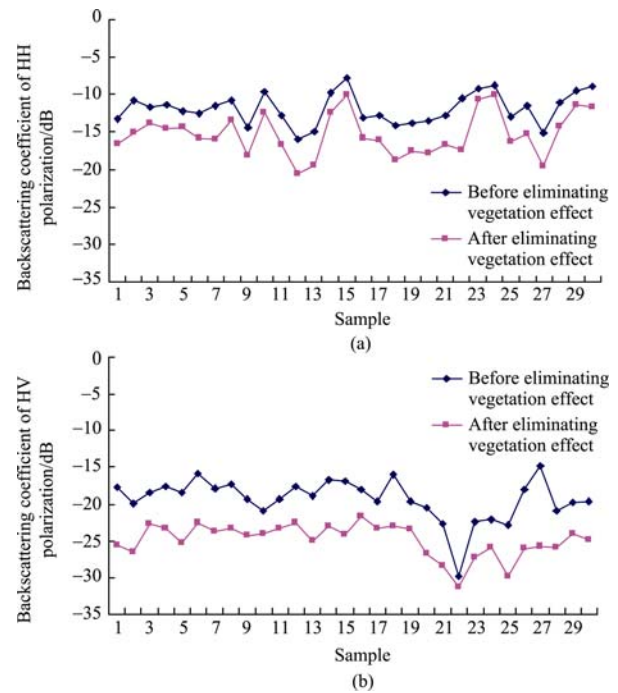


Fig. 5 Graph of relationship between HH, HV polarization backscattering coefficient
(a) HH polarization; (b) HV polarization

It is showed in Fig. 5 that, HH, HV polarization backscattering coefficient are becoming attenuation when separating the scattering and absorbing of vegetation using water-cloud model. The change of HH polarization data is thin, the reason is that the cropland of these samples is over the irrigation time and the evaporation is high, which results in lower water content of leaves and rhizome. Thus, the impact to scattering and absorbing of vegetation is tiny. HV polarization data is influenced by the scattering of plant canopy and branch. The study area is mostly covered by low crops and shrub. It is supposed that the vegetation is a orbicular scattering body covered with the earth's surface and ignoring its size, figure and the distributing character of the orientation, which results in a tiny change after removing the influence of vegetation.

The influencing analysis of vegetation on backscattering coefficient $\sigma_{\text{soil}}^0(\theta)$ of bare soil:

The backscattering coefficient of vegetation $\sigma_{\text{veg}}^0(\theta)$ is acquired from Water-Cloud model, then the contribution of vegetation's scattering and absorbing can be separated from the total backscattering of radar, and then the backscattering coefficient $\sigma_{\text{soil}}^0(\theta)$ of bare soil is obtained. The relationship between HH, HV polarization backscattering coefficient and soil water content before and after eliminating vegetation effect are respectively showed in Fig. 6 and Fig. 7.

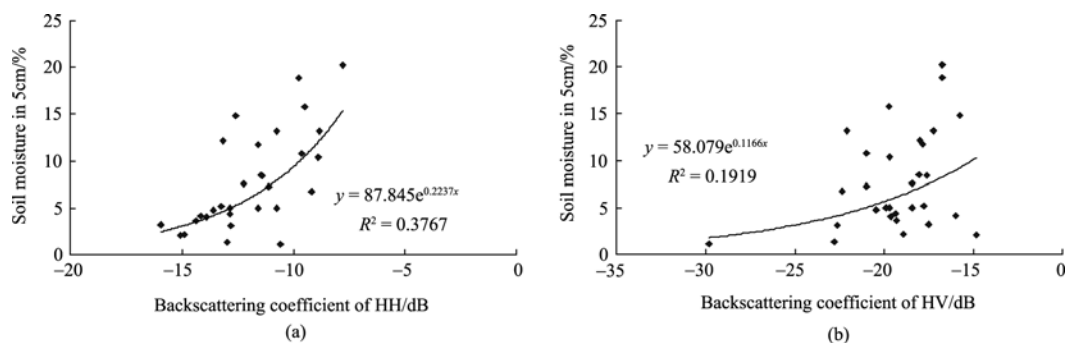


Fig. 6 Scatter plot of HH, HV polarization backscattering coefficient and soil water content before eliminating vegetation effect
(a) HH polarization; (b) HV polarization

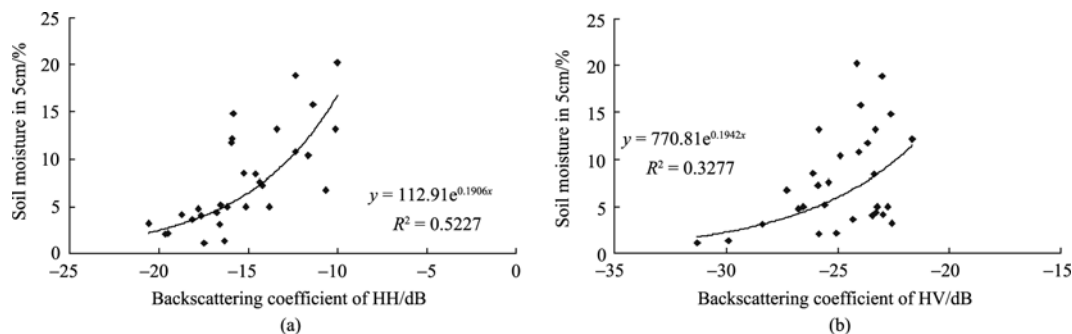


Fig. 7 Scatter plot of HH, HV polarization backscattering coefficient and soil water content after eliminating vegetation effect
(a) HH polarization; (b) HV polarization

Fig. 6 and Fig. 7 illustrate the correlation coefficient of HH, HV polarization backscattering coefficient and soil water content before eliminating vegetation effect are respectively 0.3769 and 0.1919, while they rise to 0.5227 and 0.3277 with the use of Water-Cloud Model after eliminating vegetation effect. Therefore, the relativity of soil backscattering coefficient and soil water content is increasing while eliminating the influence of vegetation. Research indicated HH polarization is much more sensitive to soil water content (Bao *et al.*, 2006), data in this paper validate that HH polarization combining with Water-Cloud Model performs well in the separation of vegetation's scattering and absorbing from the total backscattering of soil.

Based on the above conclusion, establishing the connection model of soil water content and HH polarization backscattering coefficient, the regress equation is as follows:

$$\text{Water5} = 112.91e^{0.1906\delta} \quad (R^2 = 0.5227, n = 30) \quad (12)$$

Use the Eq. (12) to retrieve the samples' soil water content, results is as Fig. 8.

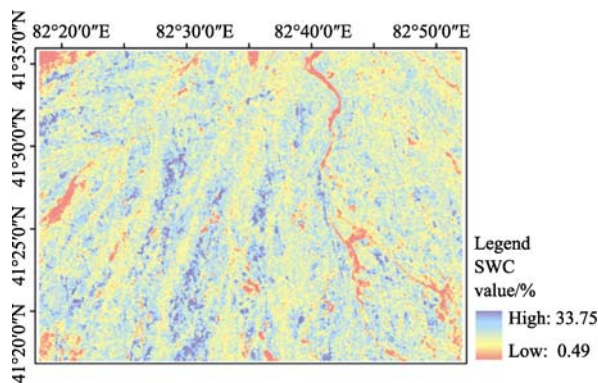


Fig. 8 Soil water content map

Field survey shows some of the river ways inside of the oasis are dry. The top left corner of the image is oasis-desert ecotone, where the soil water content is less than 8%, as the vegetation cover area is out of the irrigating time, the soil water content are mostly between 7% and 15%, and only the soil water content of a hand of marsh are a little higher. The results of field survey are consistent with the detection of the soil moisture.

5 CONCLUSION AND DISCUSSION

In this paper, a case study is the Delta oasis of Weigan and Kuqa rivers in the Xinjiang where provided with predominance of terrain characteristic. Expert the advantages of initiative microwave remote sensing Radarsat-2 data and visible remote sensing TM data to extract water content. Firstly, using TM data to extract water content of plant, then combining with Water-Cloud Model to eliminate the impact of vegetation to backscattering of soil, finally, simulating the relationship between backscattering coefficient and soil water content and validating and analysis the results, conclusions show:

(1) Comparing with soil water content data and backscattering coefficient of SAR image, visible data combining with radar data performs well to extract the information of vegetation and soil water content, and HH polarization backscattering coefficient is much closer to the change of soil water content.

(2) Years' difference has influence on character of vegetation. Although the year and the month of the soil water content data from field survey are contemporaneous with the image, the days are not, Which are likely to lead to differences of water

ingredient, leaves and rhizome water content and soil water content and them will disturb the extracting of plant water content. The continuing study can try to relatively transform the spectrum data and construct some index to eliminate the effect of exoteric factors.

(3) The hypsography in study area is flatness, and mostly covered by low plants, accordingly, the effect of surface roughness is not taken into account when calculating the soil water content. While in practical application the impact of surface roughness to radar echo is not neglected, which is a problem in this research. The continuing work is to add the analysis of the influence of surface roughness.

Presently, it has been a big progress of retrieving soil water content using microwave remote sensing, but it is also difficult to establish a universal arithmetic to retrieve soil moisture, which is mainly induced by the complexity of factors effecting microwave backscattering coefficient such as surface roughness and vegetation coverage and the uncertainty of the relationship between these factors. So how to eliminate these effects is the emphases of the continuing work and in latter research multi-source data should be comprehensively utilized and combining with kinds of retrieval model to found a regional initiative microwave remote sensing soil water content retrieval arithmetic in order to improve the precision of soil moisture inversion.

REFERENCES

- Baghdadi N, King C and Clumby A. 2002. An empirical calibration of the integral equation model based. SAR data ,soil moisture and surface roughness measurement over Bare soils. *International Journal of Remote Sensing*, **23**(20): 4325—4340
- Bao Y S, Liu L Y, Wang J H and Li X W. 2006. Estimation of soil water content and wheat coverage with ASAR image. *Journal of Remote Sensing*, **10**(3): 263—271
- Cashion J, Lakshmi V and Bosch D. 2005. Microwave remote sensing of soil moisture: evaluation of the TRMM microwave imager (TMI) satellite for the Little River Watershed Tifton, Georgia. *Journal of Hydrology*, **307**: 243—253
- Chen D Y, Huang J F and Jackson T J. 2005. Vegetation water content estimation for corn and soybeans using spectral indices derived from MODIS near- and short-wave infrared bands. *Remote Sensing of Environment*, **98**: 225—236
- Chen H L and Mao L X. 1999. A review: theories, methods and development on soil moisture monitoring by remote sensing. *Remote Sensing Technology and Application*, **14**(2): 55—65
- Chen Q, Li Z, Wang L and Wei X L. 2007. The study of estimating soil moisture using ERS wind scatterometer. *Journal of Remote Sensing*, **11**(6): 803—810
- Fung A K, Li Z Q and Chen K S. 1992. Backscattering from a randomly rough dielectric surface. *IEEE Transactions on Geoscience and Remote Sensing*, **30**(2): 356—369
- Gao B C. 1996. NDWI-A normalized difference water index for remote sensing of vegetation liquid water from space. *Remote Sensing of Environment*, **58**: 257—266
- Gao F, Wang J M, Sun C Q and Wen J. 2001. Advances in study on microwave remote sensing of soil moisture. *Remote Sensing Technology and Application*, **16**(2): 97—102
- Gao S, Niu Z and Liu C Z. 2008. The estimation of tropical plantation forest leaf area index based on Radarsat SAR data. *Remote Sensing for Land & resources*, **78**(4): 35—38
- Guo G M and Zhao B R. 2004. Monitoring soil moisture content with MODIS data. *Soils*, **36**(2): 219—221
- Jackson T J, Chen D and Cosh M. 2004. Vegetation water content mapping using Landsat data derived normalized difference water index for corn and soybeans. *Remote Sensing of Environment*, **92**: 475—482
- Liao J J, Guo H D, Shao Y, Li X W and Veneziani N. 2002. Method and model of surface feature detection in arid to Semi-arid Area Using SAR Interferometry. *Journal of Remote Sensing*, **6**(6): 431—434
- Li Z, Guo H D and Shi J C. 2002. Measuring the change of soil moisture with vegetation cover integration passive and active microwave data. *Journal of Remote Sensing*, **6**(6): 481—484
- Liu W X, Liu X L and Wang J. 2008. Remote sensing retrieval of soil moisture using ENVISAT-ASAR and MODIS images in vegetated areas of Huanan. *Agricultural Research in the Arid Areas*, **26**(3): 39—43
- Liu W, Shi J C and Wang J M. 2005. Applying the decomposition technique in vegetated surface to estimate soil moisture by multi-temporal measurements. *Remote Sensing Information*, (4): 3—6
- Liu Z H and Zhao Y S. 2002. The application study of MODTRAN and 6S model on atmospheric correction of MODIS image. *Journal of Remote Sensing*, **6**: 217—222
- Rosnay P D, Calvet J C and Kerr Y. 2006. SMOSREX: A long term field campaign experiment for soil moisture and land surface processes remote sensing. *Remote Sensing of Environment*, (102): 377—389
- Urso G D and Minacapilli M. 2006. A semi-empirical approach for surface soil water content estimation from radar data without a-priori information on surface roughness. *Journal of Hydrology*, **321**: 297—310
- Wang J and Xu R S. 2008. Methods and research developments for retrieval of vegetable water content by remote sensing. *Remote Sensing Information*, (1): 100—105
- Wickel A J, Jackson T J and Wood E F. 2001. Multitemporal monitoring of soil moisture with radarsat SAR during the 1997 Southern Great Plains hydrology experiment. *International Journal of Remote Sensing*, **22**(8): 1571—1583
- Xiong W C and Shao Y. 2006. Applying multi-temporal synthetic aperture radar (SAR) to evaluating soil-water and salt content based on IEM in arid areas. *Journal of Remote Sensing*, **10**(1): 111—117
- Xu H Q. 2008. Comment on the enhanced water index (EWI): a discussion on the creation of a water index. *Geo-Information Science*, **10**(6): 777—780
- Yuan W, Li Z Q and Liu N. 2004. Analysis of data sets with different microwave remote sensing mode in soil moisture retrieval. *Engineering Science*, **6**(6): 50—56
- Zarco-Tejada P J, Rueda C A and Ustin S L. 2003. Water content estimation in vegetation with MODIS reflectance data and model inversion methods. *Remote Sensing of Environment*, **85**: 109—124

植被覆盖地表土壤水分遥感反演

周 鹏, 丁建丽, 王 飞, 古丽加玛丽·吾不力, 张治广

新疆大学资源与环境科学学院, 省部共建新疆绿洲生态教育部重点实验室, 新疆 乌鲁木齐 830046

摘 要: 以地域特色突出的新疆渭干河-库车河三角洲绿洲为研究区, 联合使用雷达数据和光学遥感数据, 对干旱区绿洲土壤和植被水分信息进行提取。在同期光学遥感影像数据提取植被归一化差分水分指数基础上, 利用“水-云模型”从雷达数据总的后向散射中去除植被影响, 建立土壤后向散射系数与土壤含水量的关系, 相关系数为 HH 极化 $R^2=0.5227$, HV 极化 $R^2=0.3277$ 。结果表明利用 C 波段 HH 极化雷达影像数据结合光学影像数据, 进行干旱半干旱地区棉花、玉米等农作物种植区地表土壤水分反演时, 在中等覆盖条件下去除植被影响有较好的效果。

关键词: 土壤水分, 遥感, 植被, 后向散射系数, 水云模型

中图分类号: TP751.1

文献标志码: A

引用格式: 周 鹏, 丁建丽, 王 飞, 古丽加玛丽·吾不力, 张治广. 2010. 植被覆盖地表土壤水分遥感反演. 遥感学报, 14(5): 959—973

Zhou P, Ding J L, Wang F, Guljamal.Ubul and Zhang Z G. 2010. Retrieval methods of soil water content in vegetation covering areas based on multi-source remote sensing data. *Journal of Remote Sensing*, 14(5): 959—973

1 引 言

土壤水分是地球生态系统的一个非常重要的组成部分, 是联系地表水与地下水的纽带, 在全球水循环运动中扮演着非常重要的角色, 也是水文、气象和农业研究中的重要参数(袁苇等, 2004)。大面积土壤水分的监测是农业水管理以及农作物旱情预报的一个重要内容, 同时区域尺度乃至全球尺度的土壤水分信息也是陆面过程模式研究必不可少的一个参量, 对改善区域及全球气候模式预报结果起着重要的作用(高峰等, 2001)。现阶段, 区域范围尺度上的土壤水分测量有助于解决干旱区域水文模型, 农作物生长监测等方面的问题。土壤水分测量时, 传统的方法需要实地操作和繁杂的后处理过程, 不仅耗时, 而且难以获得大范围的同步的土壤水分信息, 遥感技术的发展为区域尺度的土壤水分信息的获取提供了有效手段(Cashion 等, 2005; Urso & Minacapilli, 2006)。目前, 遥感监测土壤水分主要有热惯量、热红外、作物缺水指数、距平植被指数法及

微波遥感等方法(陈怀亮等, 1999; 郭广猛&赵冰茹, 2004)。其中微波遥感具有全天时、全天候、高重复覆盖率和一定的穿透能力, 可以克服天气状况等条件的限制, 这使得微波遥感土壤水分监测较为广泛的应用到干旱半干旱地区土壤水分变化研究中。

微波遥感土壤水分监测研究经历了 30 多年的发展历史, 已建立了一些后向散射系数模型(如小扰动模型、基尔霍夫模型、双尺度模型和积分方程模型等)和经验半经验模型(Baghdadi 等, 2002; 廖静娟等, 2002; Wickel 等, 2001; 熊文成&邵芸, 2006)。但是在干旱半干旱绿洲植被覆盖地区, 受到地表粗糙度及植被覆盖的影响, 这些反演模型的应用有所限制, 因为较高的植被覆盖率会引起对土壤水分的过低估计和对表面粗糙度的过高估计(刘伟等, 2005), 这使得土壤水分信息的获取变得复杂。研究土壤水分的关键问题是消除地表粗糙度影响以及从土壤水分中分离出植被散射和吸收的贡献。在这些模型中, 植被含水量(VWC)是一个重要的参数。由于该参数大面积测量比较困难, 因此经常利用光学影像进行

收稿日期: 2009-11-20; 修订日期: 2010-04-20

基金项目: 国家自然科学基金项目(编号: 40861020); 测绘遥感信息工程国家重点实验室开放基金(编号: 09R03); 教育部科学研究重点项目以及新疆自然科学基金项目(编号: 200821128)资助。

第一作者简介: 周鹏(1980—), 男, 新疆大学资源与环境科学学院在读硕士研究生, 主要从事干旱区资源环境及遥感应用研究。E-mail: zp5226@hotmail.com。

通讯作者: 丁建丽, E-mail: watarid@xju.edu.cn。

预测,进而建立改进型归一化差分水分指数(NDMI)与 VWC 的关系。本文在光学影像数据的基础上,利用 NDMI 确定研究区的植被含水量,应用多极化星载雷达数据结合微波散射的水云模型,去除了植被层的影响,从总的后向散射系数中分离植被散射和吸收的贡献,对干旱区绿洲植被覆盖地表土壤水分的估算进行研究。

2 研究区概况与数据源

2.1 研究区概况

研究区位于塔里木盆地的中北部,渭干河-库车河流域的下游,天山南麓中部,塔克拉玛干沙漠北缘。地势北高南低,平均海拔 920—1100m,属大陆性暖温带极端干旱气候。多年平均蒸发量 2420.23mm,多年平均降水量为 43.1mm,蒸降比约为 54:1。根据实地采样点确定研究区边界坐标为:东经 82°15′—82°53′,北纬 41°15′—42°36′。研究区大部分为农业区,地表植被覆盖类型简单,较适合于地表土壤水分研究。该地区地表植被覆盖以棉花(55%)、玉米(15%)为主,伴有其他泌盐植物和盐生灌丛如怪柳、芦苇、盐穗木及骆驼刺等。

2.2 卫星数据概况

Radarsat-2 卫星于 2007-12-14 在哈萨克斯坦的拜科努尔航天发射基地成功发射,它可以提供 11 种波束模式,最高分辨率为 3m,最大成像幅宽为 500km,最大数据率为 445.4Mb/s,入射角范围为 10°—60°,工作在 C 波段能够有效地提取地表 5cm 土壤水分信息(表 1)。

表 1 Radarsat-2 系统主要参数

| 载波频率 | 极化方式 | 带宽 /MHz | 天线尺寸 /m ² | 天线质量 /kg | 有源天线 | 计划间隔度/dB |
|--------------------|-------------------------|----------------------------|----------------------|----------|------------------|----------|
| C 波段 (5.405GHz) | HH, HV, VH, VV | 11.6, 17.3, 30, 50, 100 | 15×1.5 | 750 | C-Band T/R 模块 | >25 |

雷达数据采用 Radarsat-2 二极化数据产品,极化方式为 HH/HV,影像获取时间为 2008-09-10。光学数据采用同时相的 Landsat5 TM 数据产品,内含用来计算 NDMI 的近红外和中红外波段数据。研究区影像数据如图 1 和图 2。

2.3 样品采集与分析

以 2007-09-27 的 LandSat5 TM 卫星影像数据为参考图,结合 GPS 定位技术,在渭-库绿洲中部及西

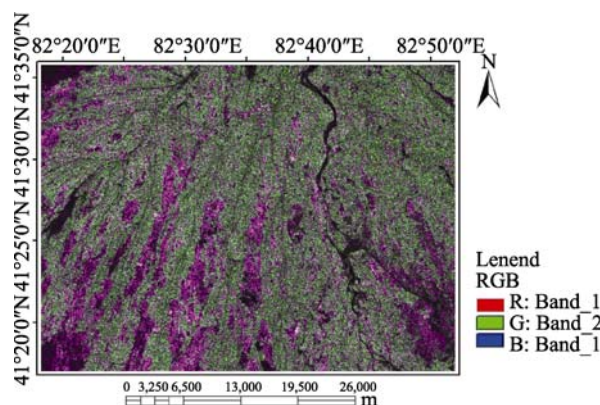


图 1 RADARSAT 2 HH/HV 极化合成影像

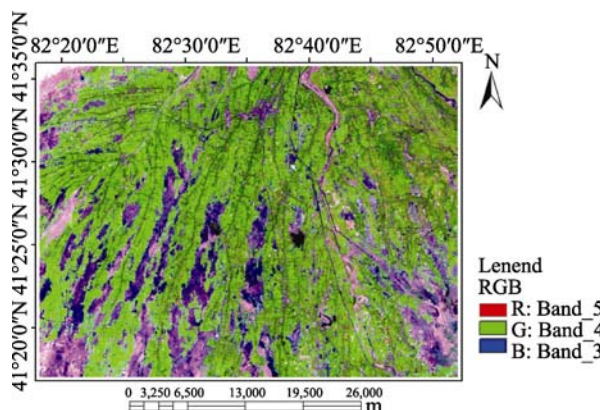


图 2 Landsat5 TM 543 波段 RGB 合成影像

南部选择典型采样区。采样时样点的分布尽可能的做到规则分布,并且综合考虑当地土质、植被类型等因素,采样的时间为 2008 年 9 月 16—26 日。定位采样点为 30 个,在定位点 30m 的范围内布置 5 个采样点,样点成梅花状分布,对每个样点进行剖面挖掘,每个样点剖面均按 0—5cm 进行采样,取得土样及部分植被样本进行封存并带回实验室,用烘干称重法获得土壤重量含水量和植被含水量数据。

3 影像数据预处理

影像数据预处理主要是针对输入的原图像进行几何校正、噪声消除、色彩增强及图像配准等。由于需要找出改进型归一化差分水分指数(NDMI)与植被含水量(VWC)的关系,所以必须对 TM 影像数据进行大气校正。而获取的 SAR 影像数据为 SLC 级数据,因此要对影像数据进行噪声消除、辐射定标和几何校正。

3.1 光学影像处理

为了保持影像光谱值的原始性,仅对影像数据

做了必要的大气校正和几何校正,以保证评价的客观性。由于大气对可见光-近红外波段和热红外波段的影响不同,因此对各波段校正需要分别进行,方法采用研究区当地较为适用的 6S 模型(刘振华&赵英时, 2002)进行大气校正。几何校正是对 TM 影像使用选择控制点的方法进行多项式校正。

3.2 雷达影像处理

3.2.1 辐射定标

由于地面散射单元同雷达之间距离不同而引起辐射误差,需要对其进行校正。

辐射定标公式为:

$$\sigma^0 = \frac{D_n^2}{K} \sin(\alpha) \quad (1)$$

式中,像元强度值为 D_n^2 ; α 是目标所在位置的雷达入射角; K 为该影像产品的绝对定标因子。 K 和 α 的值可从影像的头文件中获取。在参数选择上,采用 SIGMA 参数校正。

通过计算出图像上每一个像元的距离方向上的入射角,利用下面的定标公式可以把 Radarsat-2 卫星图像数据转换为后向散射系数如下表示:

$$\sigma^0(\theta) = 10 \log(D_n^2 / A_1) / A_2 + 10 \log(\sin(\theta)) \quad (2)$$

式中, D_n 为雷达图像的灰度值; A_1 , A_2 为雷达系统自动增益控制系数; θ 是每个像元沿距离方向上的入射角。

3.2.2 噪声处理

由于 Radarsat-2 成像过程中要做相干处理,因而形成了大量斑点(Speckle),对专题特征提取造成障碍,需要进行去噪声的处理。经过多次试验分析,利用 Gamma 滤波器对原始 SAR 图像进行滤波效果最好,可以消除大部分斑点。

3.2.3 几何校正

由于本文所用雷达影像覆盖区属平坦地区,因此采用三次多项式法加以校正。

4 植被覆盖地表土壤水分反演

首先在选择合适的微波散射模型的基础上,对植被含水量(VWC)信息进行提取。考虑到该信息大面积测量和提取有一定难度,且对地表植被覆盖具有一定的破坏性,本文利用 Landsat5 TM 影像数据计算出改进型归一化差水分指数(NDMI)并找出它与植被含水量(VWC)的关系,进而确定研究区植被含水量,再应用多极化星载雷达数据结合微波散射水云模型分离植被层对雷达后向散射的贡献,最

后对研究区土壤水分进行反演。

4.1 植被覆盖地表微波散射模型选择

在土壤水分微波遥感研究中,地表覆盖的植被层会干扰土壤的后向散射信号,因此需要建立合理的植被散射模型,在土壤水分反演算法中去除植被层的影响。国外很多学者对植被散射模型做过研究:美国密歇根大学的研究小组,于 1990 年提出了“MIMICS”模型(Fung 等, 1992),该模型主要针对乔木等高大植被覆盖地表建立,它考虑了植被的冠层、树干及底层地表 3 个层次,较为真实地模拟植被覆盖地表微波后向散射。而 Attma 和 Ulaby 等以农作物为研究对象,早在 1978 年就提出了“Water-Cloud”模型,该模型假定植被层为一个各向均质散射体,忽略了植被层及地表之间的相互多次散射,将植被覆盖地区总的后向散射简单的描述为两部分,即由植被直接反射回来的体散射项,以及经作物双次衰减后地面的后向散射项。由于研究区内多为棉花等低矮的作物植被覆盖,使用很少参数的“Water-Cloud”模型更为简单实用。

水云模型表述如下:

$$\sigma_{\text{can}}^0(\theta) = \sigma_{\text{veg}}^0(\theta) + \gamma^2(\theta) \sigma_{\text{soil}}^0(\theta) \quad (3)$$

式中, $\sigma_{\text{can}}^0(\theta)$ 为植被覆盖地表下总的雷达后向散射系数, $\sigma_{\text{veg}}^0(\theta)$ 为直接植被层的后向散射系数, $\sigma_{\text{soil}}^0(\theta)$ 为直接地表后向散射系数, $\gamma^2(\theta)$ 为雷达波穿透农作物层的双层衰减因子,其中:

$$\sigma_{\text{veg}}^0(\theta) = A \cdot m_{\text{veg}} \cdot \cos(\theta) \cdot (1 - \gamma^2(\theta)) \quad (4)$$

$$\gamma^2(\theta)_{\text{pp}}^2 = \exp(-2Bm_{\text{veg}} \sec(\theta)) \quad (5)$$

式中, A 和 B 分别为依赖于植被类型的参数,可以用“MIMICS”模型进行地表参数模拟,再通过回归算法获得。 m_{veg} 是植被含水量(kg/m^3), θ 为雷达波入射角。

4.2 特征参数提取及植被含水量计算

植被含水量(VWC)定义为单位面积植被中水的重量,作为“Water-Cloud”模型的重要输入参数在植被覆盖地区土壤水分反演中起到重要的作用(刘万侠等, 2008)。利用光学影像反演区域植被含水量的研究比较成熟,建立的光谱指数与 VWC 相关性较高(Jackson 等, 2004; Rosnay 等, 2006; 王洁等, 2008)。本次研究采用光学遥感反演辅以样点实测数据验证的方法计算研究区植被含水量。考虑到土壤、植被和水体在 $0.8-1.7\mu\text{m}$ 的波谱特征,选择了与实地采样时间同期的 2008-09-16 Landsat5 TM 数据,

它包含近红外和中红外波段: 波段 4(0.76 μm)、波段 5 (1.55 μm), 光谱带宽分别为 25 nm 和 20 nm, 利用植物在近红外波段具有较高的反射率, 而在中红外波段由于植物叶子水分的吸收作用导致反射率降低的特点, 运用改进型归一化植被水分指数 NDMI (Gao, 1996; Zarco-Tejada 等, 2003), 提取植被水分信息。由于研究区多为棉花及低矮盐生植被覆盖, 根据相关研究(Chen 等, 2005), 建立方程式形式如式(6), 根据实测植被含水量与 NDMI 间的关系, 建立式(7)确定 VWC 值。

$$\text{NDMI}=(\text{NIR}-\text{MIR})/(\text{NIR}+\text{MIR}) \quad (6)$$

$$\text{VWC}=2.15\text{NDMI}+0.32 \quad (7)$$

研究区内有河流、湖泊及水库, 这些水体会对植被水分信息提取造成干扰, 因此在利用遥感影像数据提取植被水分信息过程中, 必须去除这些纯水体的影响。这里选择 MNDWI 指数(徐涵秋, 2008), 根据当地情况稍加改进来提取纯水体信息, 表达式如下:

$$\text{MNDWI}=(1+0.5)(\text{GREEN}-\text{MIR})/(\text{GREEN}+\text{MIR}) \quad (8)$$

提取了纯水体信息后, 对原始图像进行掩膜处理, 去除了纯水体的影响, 经分析验证表明运用 NDMI 提取植被水分信息效果较好。

4.3 植被覆盖地表后向散射计算

主动微波遥感估算土壤水分主要受植被覆盖和地表粗糙度影响, 植被覆盖土壤表面的后向散射包括来自植被的体散射、来自地表的面散射和植被与地表间的交互作用散射项, 估算地表土壤水分需要考虑这些因素(李震等, 2002)。由于研究区内地势平坦, 多为低矮植被覆盖, 因此在计算土壤后向散射系数时较多考虑植被覆盖而忽略地表粗糙度影响。

估算土壤水分时要消除植被覆盖影响需要应用“Water-Cloud”模型去除植被层在土壤水分后向散射中的贡献。模型中参数 A 、 B 是经验常数, 具有很大的地域性, 在进行参数标定时采用目前比较成熟的方法(陈权等, 2007; 高帅等, 2008)。首先用水云模型与 MIMICS 模型对研究区植被覆盖地表的后向散射情况进行模拟, 以得到地表直接散射、地表体散射随入射角的变化关系。随后对研究区特定的建群植物进行参数化如表 2, 用 MIMICS 模型对其模拟, 在模拟结果的基础上通过非线性最小二乘法对水云模型中所涉及的植被参数 A 和 B 进行标定。

经过回归分析后得到参数 $A=0.0019$, $B=0.137$, 将其带入式(4)与式(5), 运用水云模型消除植被覆盖

表 2 MIMICS 模型模拟所需参数

| 类别 | 参数 | 数值 |
|-------|------------------------|-------|
| 传感器参数 | 频率/GHz | 5.4 |
| | 极化方式 | HH/HV |
| 地表参数 | 含水量 | 0.17 |
| | 均方根高度/cm | 0.817 |
| | 相关长度/cm | 7.528 |
| 叶片参数 | 含水量 | 0.39 |
| | 半径/cm | 2.6 |
| | 厚度/cm | 0.04 |
| | 高度/m | 0.9 |
| 枝干参数 | 半径/cm | 0.3 |
| | 长度/cm | 21 |
| | 密度/ m^3 | 8.6 |
| 环境参数 | 温度/ $^{\circ}\text{C}$ | 22 |

影响从而得到裸土后向散射, 表示如下:

$$\sigma_{\text{veg}}^0(\theta) = 0.0019m_{\text{veg}} \cos(\theta)(1-\gamma(\theta)^2) \quad (9)$$

$$\gamma^2(\theta) = \exp(-2 \times 0.137m_{\text{veg}} \sec(\theta)) \quad (10)$$

$$\sigma_{\text{soil}}^0(\theta) = \frac{\sigma^0(\theta) - \sigma_{\text{veg}}^0(\theta)}{\gamma^2(\theta)} \quad (11)$$

通过式(2)与式(11)可以计算出研究区地表总的后向散射系数与去除植被覆盖影响后的土壤后向散射系数。为了明确 HH、HV 极化数据间的关系, 这里分别做了两个极化数据的后向散射系数在地表植被覆盖影响去除前后的相关分析, 由于一些高植被覆盖区域, 土壤水分的变化不能有效的从雷达后向散射系数变化中得到反映, 因此在分析时删去了这些歧义点, 其结果见图 3 和图 4。

由图 3、图 4 可知, 无论是在地表植被覆盖影响去除之前或是之后, HH 与 HV 极化后向散射系数之间的相关系数都很低, 分别为 $R^2=0.2534$ 与 $R^2=0.2884$ 。因此研究将对 HH、HV 极化数据反演土壤水分进行讨论。

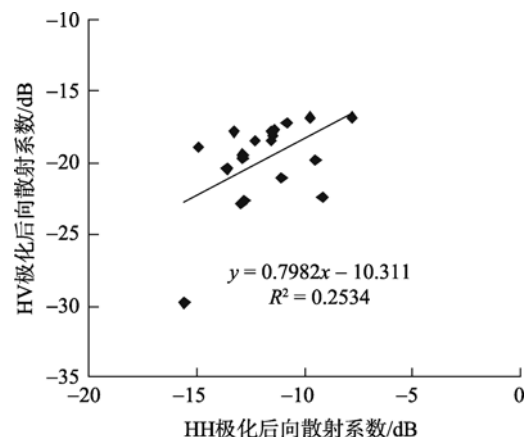


图 3 去除植被影响前 HH、HV 极化后向散射系数拟合关系图

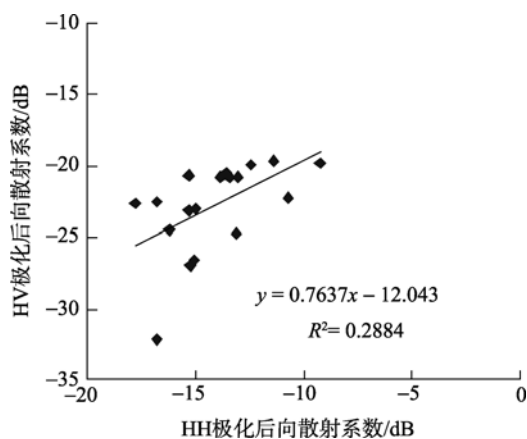


图4 去除植被影响后 HH、HV 极化后向散射系数拟合关系图

4.4 实测样点数据分析

为分析植被覆盖地表后向散射系数的影响因素,经过实地采样获得了 30 个样点 0—5cm 土层的土壤重量含水量数据并记录采样点坐标,建立与样点坐标对应的后向散射系数和实测土壤重量含水量图表(表 3)。基于表 3 数据,分析地表植被覆盖去除前后 HH、HV 极化后向散射系数与土壤含水量之间的关系,进而探讨植被覆盖对后向散射系数的影响。

表 3 采样点土壤后向散射系数和土壤重量含水量

| 样点代号 | HH 极化/dB | HV 极化/dB | 5cm 深含水量/% |
|------|----------|----------|------------|
| C 1 | -13.2507 | -17.7713 | 5.1470 |
| C 2 | -10.7600 | -19.8877 | 4.9754 |
| C 3 | -11.5946 | -18.4416 | 5.0036 |
| C 4 | -11.3997 | -17.6153 | 8.4150 |
| C 5 | -12.2587 | -18.4515 | 7.6217 |
| C 6 | -12.5959 | -15.7758 | 14.7993 |
| C 7 | -11.5938 | -17.8194 | 11.7455 |
| C 8 | -10.7801 | -17.2293 | 13.1799 |
| C 9 | -14.3954 | -19.3163 | 3.6656 |
| C 10 | -9.6117 | -21.0139 | 10.7864 |
| C 11 | -12.8598 | -19.3812 | 4.3598 |
| C 12 | -15.9316 | -17.5230 | 3.2380 |
| C 13 | -14.9207 | -18.9558 | 2.2208 |
| C 14 | -9.7728 | -16.7673 | 18.8682 |
| C 15 | -7.8132 | -16.7763 | 20.1818 |
| C 16 | -13.1535 | -17.9993 | 12.1819 |
| C 17 | -12.8540 | -19.6966 | 4.9591 |
| C 18 | -14.1582 | -16.0084 | 4.1625 |
| C 19 | -13.8883 | -19.6414 | 4.0697 |
| C 20 | -13.5933 | -20.4478 | 4.8147 |
| C 21 | -12.8223 | -22.6523 | 3.1433 |
| C 22 | -10.5719 | -29.8080 | 1.1135 |
| C 23 | -9.2110 | -22.3394 | 6.7921 |
| C 24 | -8.8493 | -22.0768 | 13.1973 |
| C 25 | -12.9640 | -22.8122 | 1.3152 |
| C 26 | -11.4630 | -18.0514 | 8.5359 |
| C 27 | -15.0914 | -14.8482 | 2.0410 |
| C 28 | -11.0910 | -20.9843 | 7.2859 |
| C 29 | -9.4889 | -19.7483 | 15.7987 |
| C 30 | -8.8780 | -19.6783 | 10.3772 |

根据 30 个采样点的坐标,获得图像上相应点的后向散射系数,拟合地表植被覆盖去除前后 HH、HV 极化后向散射系数关系如图 5。

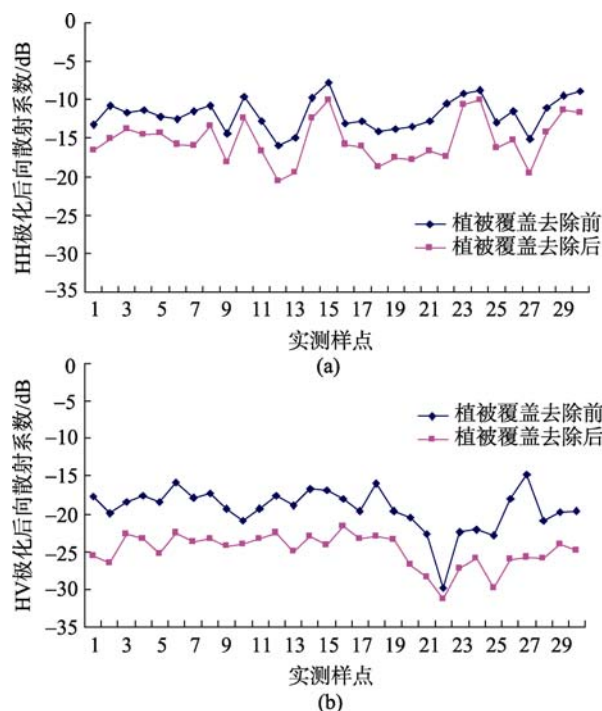


图5 后向散射系数关系图

(a) HH 极化; (b) HV 极化

由图 5 可知,在利用水云模型分离出植被层散射和吸收的贡献后,地表 HH、HV 极化后向散射系数均有衰减。HH 极化数据变化幅度不大的原因是由于样点作物所处农田已过灌溉期且当地蒸发量较大,植被叶面及根茎所含水分较低,因此植被层对后向散射的吸收及散射影响较少。而 HV 极化数据受植被冠层及枝干体散射影响较大,本次研究选择的实验区大多由低矮农作物或灌丛覆盖,选择模型时假设植被层为覆盖地表之上的一层球形散射体,没有考虑其大小、形状、朝向的分布特征,因此在去除植被层影响后数据变化幅度也不大。

地表植被覆盖对裸土后向散射系数 $\sigma_{\text{soil}}^0(\theta)$ 影响分析:

各试验点的植被后向散射系数 $\sigma_{\text{veg}}^0(\theta)$ 利用“Water-Cloud”模型计算得出,这样可以从雷达总的后向散射中分离出植被散射和吸收的贡献,得到裸土的后向散射系数 $\sigma_{\text{soil}}^0(\theta)$,并建立与土壤重量含水量之间的关系。拟合后相关系数如图 6 和图 7。

如图 6 和图 7 所示,在去除地表植被覆盖影响前,HH、HV 极化后向散射系数与土壤含水量之间的相关系数分别为 $R^2=0.3767$ 与 $R^2=0.1919$ 。利用“Water-Cloud”模型去除植被影响后两者的相关系数

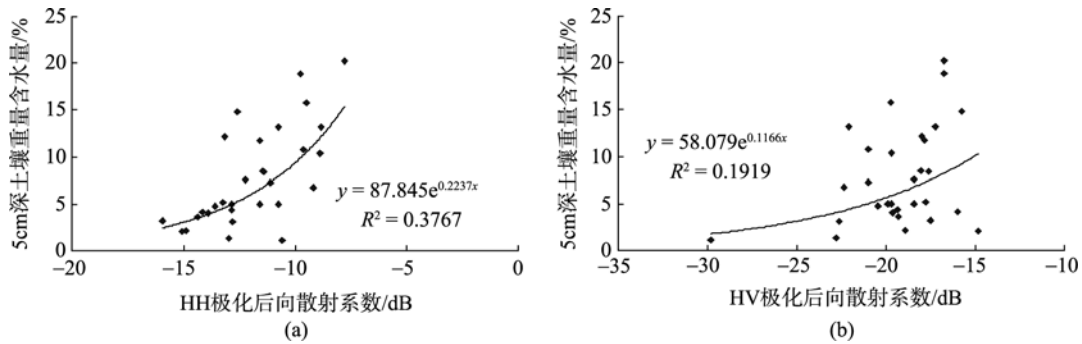


图 6 去除植被影响前后向散射系数与土壤含水量散点图
(a) HH 极化; (b) HV 极化

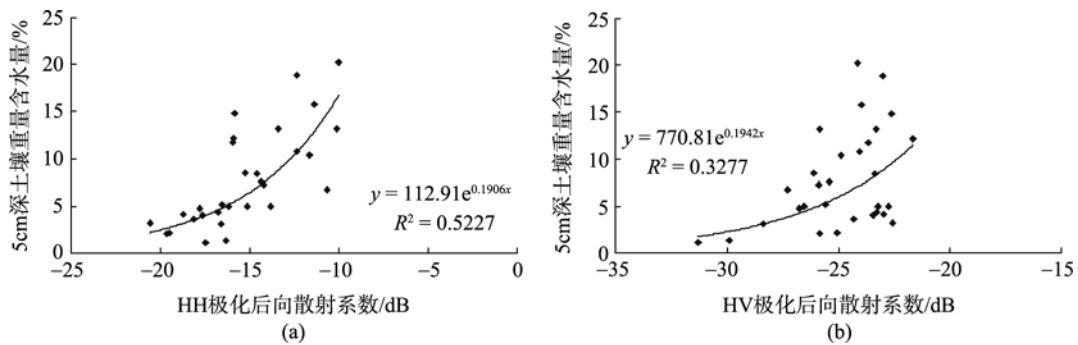


图 7 去除植被影响后, 后向散射系数与土壤含水量散点图
(a) HH 极化; (b) HV 极化

提升到 $R^2=0.5227$ 与 $R^2=0.3277$ 。由此可知, 土壤的后向散射系数与土壤含水量的相关性随着地表植被影响去除而增加, 根据已有研究(鲍艳松等, 2006), 水平同极化对土壤含水量的差异更为敏感, 参照文中数据分析结果说明利用 HH 极化数据结合水云模型较好的分离出土壤总的后向散射中植被层散射和吸收的贡献。

基于以上结论, 建立 5cm 深土壤含水量和 HH 极化后向散射系数的关系模型, 其回归方程为:

$$\text{Water}_5 = 112.91e^{0.1906\delta} \quad (R^2=0.5227, n=30) \quad (12)$$

拟合曲线如图 7, 使用式(12)对样点 5cm 深土壤重量含水量进行反演, 结果如图 8。

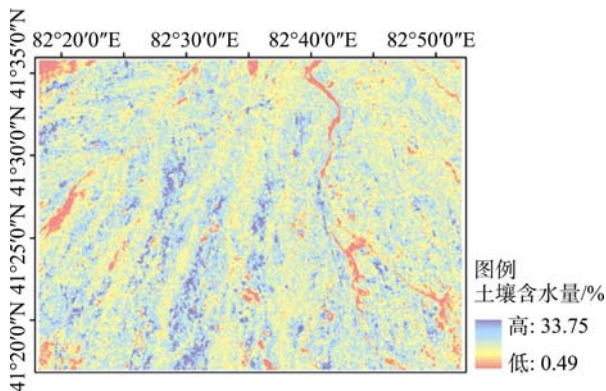


图 8 土壤含水量图

经过实地调查: 绿洲内部河道部分已经干涸, 左上角为绿洲荒漠交错地区, 土壤含水量不到 8%, 而植被覆盖区也已过灌溉期, 地表土壤含水量大多在 7%—15%, 只有少数湿地含水量较高。这一调查和土壤含水量反演结果一致。

5 结论与讨论

本文以地域特色突出的新疆渭库绿洲作为试验区, 发挥主动微波遥感 Radarsat-2 数据与光学遥感 TM 数据各自在提取水分信息上的优势, 首先由 TM 数据获取植被含水量信息, 再利用“Water-Cloud”模型去除植被覆盖对土壤后向散射的影响, 最后拟合后向散射系数与实测土壤重量含水量之间的关系并对结果进行验证与分析, 结果如下:

(1) 对比土壤重量含水量数据和 SAR 影像后向散射系数可知: 光学数据结合雷达数据在提取植被与土壤水分信息时效果较好, 其中水平同极化后向散射系数比较真实的反映土壤含水量变化。

(2) 年差对土壤质地及植被性状特征有一定的影响。研究中实测的土壤水分数据时间与影像获取时间尽管年份月份相同, 但是在天数上没有同步, 这就导致水体组成成分、植被叶面和根茎水分的含

量、土壤含水量的一些差异,这些会干扰植被水分信息的提取。后续研究中可以尝试对光谱数据进行相对变换以及构造一些指数的方法来消除外界因子影响。

(3) 研究区内地势平坦,多为低矮植被覆盖,因此在计算土壤后向散射系数时没有考虑地表粗糙度的影响。但实际应用中,地表粗糙度对雷达回波的影响是不可忽视的,这是研究中存在的问题。因此在下一步工作中,需要加入对地表粗糙度影响的分析。

目前,微波遥感反演土壤水分的研究有了很大的发展,然而要建立通用的土壤水分反演算法还比较困难。这是由于影响微波后向散射系数的各种因素如地表粗糙度及植被覆盖的复杂性,以及各影响因素之间关系的不确定性所造成的。因此如何消除这些因素对反演土壤水分的影响是接下来研究工作的重点。在后续工作中可以综合利用多种数据源,复合各种不同的反演模型来建立符合区域性特点的主动微波遥感土壤水分反演算法,进而提高土壤水分反演的精度。

REFERENCES

- Baghdadi N, King C and Clumsey A. 2002. An empirical calibration of the integral equation model based. SAR data, soil moisture and surface roughness measurement over Bare soils. *International Journal of Remote Sensing*, **23**(20): 4325—4340
- Bao Y S, Liu L Y, Wang J H and Li X W. 2006. Estimation of soil water content and wheat coverage with ASAR image. *Journal of Remote Sensing*, **10**(3): 263—271
- Cashion J, Lakshmi V and Bosch D. 2005. Microwave remote sensing of soil moisture: evaluation of the TRMM microwave imager (TMI) satellite for the Little River Watershed Tifton, Georgia. *Journal of Hydrology*, **307**: 243—253
- Chen D Y, Huang J F and Jackson T J. 2005. Vegetation water content estimation for corn and soybeans using spectral indices derived from MODIS near-and short-wave infrared bands. *Remote Sensing of Environment*, **98**: 225—236
- Chen H L, Mao L X and Feng D Y. 1999. A review: theories, methods and development on soil moisture monitoring by remote sensing. *Remote Sensing Technology and Application*, **14**(2): 55—65
- Chen Q, Li Z, Wang L and Wei X L. 2007. The study of estimating soil moisture using ERS wind scatterometer. *Journal of Remote Sensing*, **11**(6): 803—810
- Fung A K, Li Z Q and Chen K S. 1992. Backscattering from a randomly rough dielectric surface. *IEEE Transactions on Geoscience and Remote Sensing*, **30**(2): 356—369
- Gao B C. 1996. NDWI-A normalized difference water index for remote sensing of vegetation liquid water from space. *Remote Sensing of Environment*, **58**: 257—266
- Gao F, Wang J M, Sun C Q and Wen J. 2001. Advances in study on microwave remote sensing of soil moisture. *Remote Sensing Technology and Application*, **16**(2): 97—102
- Gao S, Niu Z and Liu C Z. 2008. The estimation of tropical plantation forest leaf area index based on Radarsat SAR data. *Remote Sensing for Land & resources*, **78**(4): 35—38
- Guo G M and Zhao B R. 2004. Monitoring soil moisture content with MODIS data. *Soils*, **36**(2): 219—221
- Jackson T J, Chen D and Cosh M. 2004. Vegetation water content mapping using Landsat data derived normalized difference water index for corn and soybeans. *Remote Sensing of Environment*, **92**: 475—482
- Liao J J, Guo H D, Shao Y, Li X W and Veneziani N. 2002. Method and model of surface feature detection in arid to Semi-arid Area Using SAR Interferometry. *Journal of Remote Sensing*, **6**(6): 431—434
- Li Z, Guo H D and Shi J C. 2002. Measuring the change of soil moisture with vegetation cover integration passive and active microwave data. *Journal of Remote Sensing*, **6**(6): 481—484
- Liu W X, Liu X L and Wang J. 2008. Remote sensing retrieval of soil moisture using ENVISAT-ASAR and MODIS images in vegetated areas of Huanan. *Agricultural Research in the Arid Areas*, **26**(3): 39—43
- Liu W, Shi J C and Wang J M. 2005. Applying the decomposition technique in vegetated surface to estimate soil moisture by multi-temporal measurements. *Remote Sensing Information*, (4): 3—6
- Liu Z H and Zhao Y S. 2002. The application study of MODTRAN and 6S model on atmospheric correction of MODIS image. *Journal of Remote Sensing*, **6**(Supplement): 217—222
- Rosnay P D, Calvet J C and Kerr Y. 2006. SMOSREX: A long term field campaign experiment for soil moisture and land surface processes remote sensing. *Remote Sensing of Environment*, **102**: 377—389
- Urso G D and Minacapilli M. 2006. A semi-empirical approach for surface soil water content estimation from radar data without a-priori information on surface roughness. *Journal of Hydrology*, **321**: 297—310
- Wang J, Xu R S, Ma Y L, Cai R, Miao L and Chen Y. 2008. Methods and research developments for retrieval of vegetable water content by remote sensing. *Remote Sensing Information*, (1): 100—105
- Wickel A J, Jackson T J and Wood E F. 2001. Multitemporal monitoring of soil moisture with Radarsat SAR during the 1997 Southern Great Plains hydrology experiment. *International*

Journal of Remote Sensing, **22**(8): 1571—1583

- Xiong W C and Shao Y. 2006. Applying multi-temporal synthetic aperture radar(SAR) to evaluating soil-water and salt content based on IEM in arid areas. *Journal of Remote Sensing*, **10**(1): 111—117
- Xu H Q. 2008. Comment on the enhanced water index(EWI): a discussion on the creation of a water index. *Geo-Information Science*, **10**(6): 777—780
- Yuan W, Li Z Q and Liu N. 2004. Analysis of data sets with different microwave remote sensing mode in soil moisture retrieval. *Engineering Science*, **6**(6): 50—56
- Zarco-Tejada P J, Rueda C A and Ustin S L. 2003. Water content estimation in vegetation with MODIS reflectance data and model inversion methods. *Remote Sensing of Environment*, **85**: 109—124
- 附中文参考文献**
- 鲍艳松, 刘良云, 王纪华, 李小文. 2006. 利用 ASAR 图像监测土壤含水量和小麦覆盖度. *遥感学报*, **10**(3): 263—271
- 陈怀亮, 毛留喜, 冯定原. 1999. 遥感监测土壤水分的理论、方法及研究进展. *遥感技术与应用*, **14**(2): 55—65
- 陈权, 李震, 王磊, 魏小兰. 2007. 用 ERS 风散射计数据估算土壤水分方法的研究. *遥感学报*, **11**(6): 803—810
- 高峰, 王介民, 孙成权, 文军. 2001. 微波遥感土壤湿度研究进展. *遥感技术与应用*, **16**(2): 97—102
- 高帅, 牛铮, 刘晨洲. 2008. 基于 RADARSAT SAR 估测热带人工林叶面积指数研究. *国土资源遥感*, **78**(4): 35—38
- 郭广猛, 赵冰茹. 2004. 使用 MODIS 数据监测土壤湿度. *土壤学报*, **36**(2): 219—221
- 廖静娟, 郭华东, 邵芸, 李新武, Venezianin. 2002. 干旱-半干旱地区地表特征探测的成像雷达干涉测量方法与模型. *遥感学报*, **6**(6): 431—434
- 李震, 郭华东, 施建成. 2002. 综合主动和被动微波数据监测土壤水分变化. *遥感学报*, **6**(6): 481—484
- 刘万侠, 刘旭拢, 王娟, 曾文华. 2008. 华南农作物覆盖区土壤水分 ENVISAT-ASAR 与 MODIS 数据联合反演算法研究. *干旱区农业研究*, **26**(3): 39—43
- 刘伟, 施建成, 王建明. 2005. 极化分解技术在估算植被覆盖地区土壤水分变化中的应用. *遥感信息*, (4): 3—6
- 刘振华, 赵英时. 2002. MODIS 图像大气校正中 MODTRAN 与 6S 模型的应用研究. *遥感学报*, **6**(增刊): 217—222
- 王洁, 徐瑞松, 马跃良, 蔡睿, 苗莉, 陈戡. 2008. 植被含水量的遥感反演方法及研究进展. *遥感信息*, (1): 100—105
- 熊文成, 邵芸. 2006. 基于 IEM 模拟的干旱区多时相数据含水量盐量反演模型及分析. *遥感学报*, **10**(1): 111—117
- 徐涵秋. 2008. 从增强型水体指数分析遥感水体指数的创建. *地球信息科学*, **10**(6): 777—780
- 袁苇, 李宗谦, 刘宁. 2004. 不同微波遥感模态和不同数据组合的等湿度区域分布与土壤湿度的反演. *中国工程科学*, **6**(6): 50—56